Brassinosteroid signaling and auxin transport are required to establish the periodic pattern of *Arabidopsis* shoot vascular bundles

Marta Ibañes[a], Norma Fàbregas[b], Joanne Chory[c,1], and Ana I. Caño-Delgado[b,1]

[a]Departament Estructura i Constituents de la Matèria, Universitat de Barcelona, Diagonal 647, 08028 Barcelona, Spain; [b]Molecular Genetics Department, Centre for Research in Agricultural Genomics (CSIC-IRTA-UAB), C/Jordi Girona 18-24, 08034 Barcelona, Spain; and [c]Howard Hughes Medical Institute and Plant Biology Laboratory, The Salk Institute for Biological Studies, 10010 North Torrey Pines Road, La Jolla, CA 92037

The plant vascular system provides transport and support capabilities that are essential for plant growth and development, yet the mechanisms directing the arrangement of vascular bundles within the shoot inflorescence stem remain unknown. We used computational and experimental biology to evaluate the role of auxin and brassinosteroid hormones in vascular patterning in *Arabidopsis*. We show that periodic auxin maxima controlled by polar transport and not overall auxin levels underlie vascular bundle spacing, whereas brassinosteroids modulate bundle number by promoting early procambial divisions. Overall, this study demonstrates that auxin polar transport coupled to brassinosteroid signaling is required to determine the radial pattern of vascular bundles in shoots.

mathematical model | pattern formation | plant hormones | procambium

The variety and complexity of vascular patterns among plant species have attracted the attention of both biologists and mathematicians for many years (1–5). In the *Arabidopsis* shoot, the vascular pattern is set up in embryogenesis by asymmetric divisions of the procambium cells (6). After germination, subsequent procambial cell division and differentiation gives rise to the xylem, the water conducting tissues, and the phloem, through which photosynthetic compounds and signaling molecules are transported (7, 8). This primary provascular growth derives from the activity of primary plant growth and serves as a vascular template along plant development (1). The vasculature forms a continuous apico-basally connected structure along the plant shoot. At the base of the main inflorescence stem of wild-type (WT) plants, the completion of primary provascular growth is observed. Procambial cells have produced functional xylem and phloem forming a vascular bundle (VB) and differentiated interfascicular fibers (IF) in between bundles (Fig. 1*A*). IFs are composed of 3 to 4 layers of fiber cells and are mostly responsible for the mechanical strength of the mature stem (9). The procambium places xylem centripetally and phloem centrifugally, contributing to the formation of collateral VBs (1) (Fig. 1*B*). Across a cross-section, the stem vasculature exhibits a radial organization made by the periodic alternation of VBs with the IF in between, together forming the vascular ring (Fig. 1*A*).

Genetic studies have identified a number of vascular patterning mutants (2, 10–12), but the mechanisms underlying VB pattern formation are still unknown. Two plant hormones, auxin and brassinosteroids (BRs), have been implicated in vascular differentiation. Auxin is essential for vascular tissue formation and differentiation (13, 14). In leaves, it has been shown that auxin accumulates in the procambial cells (15, 16), leading to the gradual canalization of auxin into the leaf vascular strands through polarization of auxin efflux carriers (4, 5, 17). In the shoot, it has been shown that the auxin efflux carrier PIN1 is expressed in the procambium and xylem cells, at the basal side and in a fraction of the lateral cell membranes (18). Mutations in *pin1* or chemical inhibition of auxin transport with naphthalene acetic acid (NPA)

induces a dramatic increase of differentiated xylem cells, which expand the VBs along the ring adjacent to cauline leaves (18, 19). Altogether these results raise the intriguing question of how auxin is participating in shoot-VB patterning.

Brassinosteroids, the steroid hormones of plants, play a major role in promoting cell expansion, and a signaling pathway that controls cell expansion has been elucidated (20). BRs are also involved in vascular cell differentiation of vegetative organs. In *Zinnia* mesophyll cell cultures, BRs have been shown to regulate xylem differentiation (21–23). Moreover, a number of BR mutants of rice (24) and *Arabidopsis* (25–27) show various vascular differentiation defects; however, a full characterization of the alterations induced by BRs on the periodic VB pattern in *Arabidopsis* shoots is lacking and the mechanism by which BRs contribute to this patterning is not yet understood.

The goal of this study is to examine the roles of auxin and BRs in vascular patterning in the shoot inflorescence stem. Because the *Arabidopsis* shoot is not as amenable to studies of auxin polar transport as leaves and the shoot apical meristem, we used a systems biology approach. By means of a mathematical and computational model and quantitative experimental data, we show that BR signaling and auxin polar transport, not auxin levels, are required to set the number and arrangement of plant-shoot vasculature.

Results and Discussion

Schematically, the shoot vascular pattern can be decomposed into circularly and periodically distributed vascular units, each of which consists of a VB and the clockwise adjacent IF (Fig. 1*C*). Whereas incipient xylem differentiating cells appear spaced across a ring-like geometry at the shoot apex (at ≈100 μm below the apex; see Fig. S1 *A–D*), the periodic pattern of differentiated VBs is set up at ≈2 cm below the apex being maintained along the inflorescence stem (Fig. S1 *E–G*).

Recently, auxin polar transport has been shown to be critical to position organs periodically through auxin maxima during the emergence of organ primordia in the shoot, such as the axillary meristems and leaves during the generation of phyllotactic patterns (28, 29). In this context, we hypothesized that auxin maxima promote xylem differentiation and the formation of VBs in the shoot and we investigated whether a periodic distribution of auxin maxima can underlie the formation (i.e., number and positioning) of primary VBs along the shoot vascular ring. To this end, we first
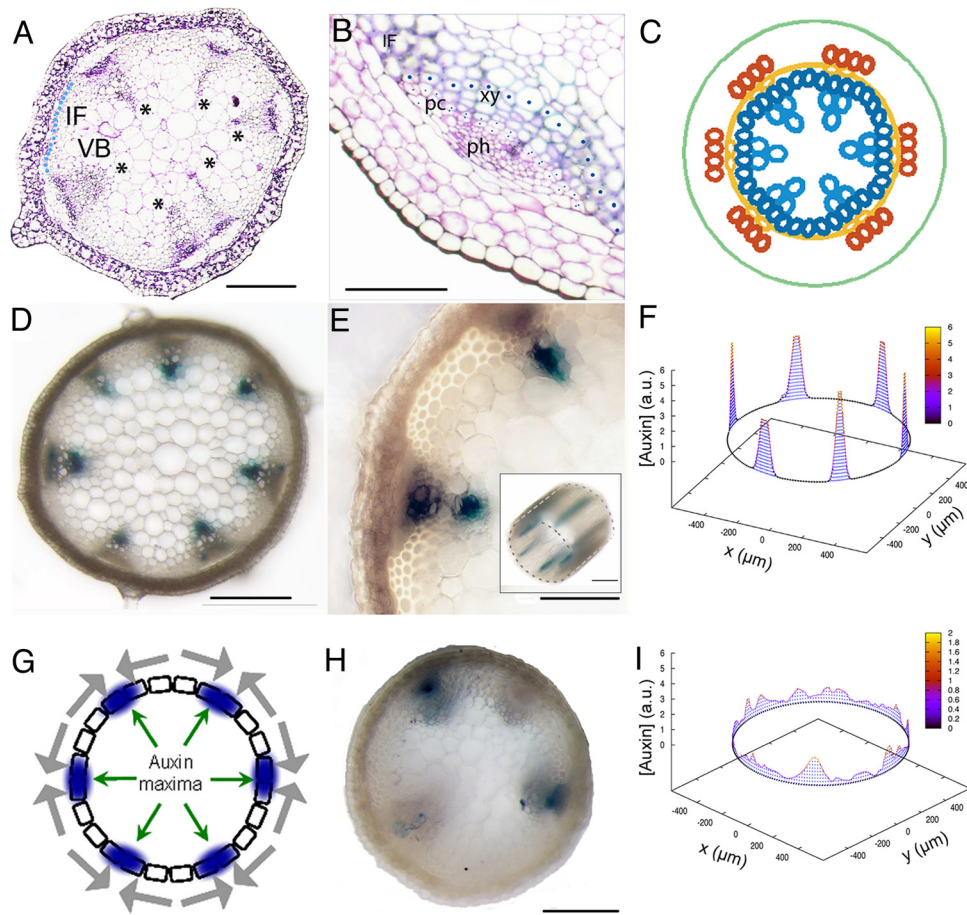

Fig. 1. A model for VB spacing in the *Arabidopsis* shoot inflorescence stem. (*A*) *Arabidopsis* Col-0 WT transverse-section at the base of the inflorescence stem. IF at the base of the vascular ring (light blue circles) depicted as measured. Asterisks denote VBs. (*B*) Magnification of a VB. Procambial and xylem cells at the base of the vascular ring depicted as measured. Procambial cells (pc), xylem (xy) and phloem (ph) forming a VB and interfascicular fiber (IF) in between. (*C*) Primary VB pattern scheme. Yellow, procambium; blue, xylem and IF; orange, phloem. (*D* and *E*) Radial view of DR5::GUS expression at the base of the inflorescence (*D*) and in a VB (*E*) for the WT. *Inset* in *E* shows a translongitudinal view showing the continuous and periodic expression of DR5::GUS along the shoot inflorescence stem. (*F*) Numerical simulation results for auxin concentration ([Auxin]) in arbitrary units (a.u.) along a ring of N_F = 210 cells arising from a pool of N_i = 120 progenitors (see Fig. S2 for parameter values). *x* and *y* stand for spatial coordinates (WT average diameter used). (*G*) Auxin maxima (blue), driven by polar transport (gray arrows, plotted outside cells for clarity), position VBs along the vascular ring of cells (boxes). (*H*) Radial view of DR5::GUS expression at the base of the inflorescence for a NPA-treated plant. (*I*) Simulated auxin concentration across a ring of cells as in *F* when the efflux permeabilities are decreased by a factor of 100. [Scale bars: 200 μm (*A* and *D*) and 100 μm (*B* and *E*).]

evaluated whether auxin maxima coincide with VBs. We analyzed the expression pattern of a synthetic auxin-response element DR5::GUS, which has been used as a read-out of auxin levels (30). At the base of the inflorescence stem, where completion of the pattern is observed, β-glucuronidase (GUS) activity appeared specifically at the vascular bundles, having a periodic expression in the procambial and differentiating xylem cells (Fig. 1 *D* and *E*). This result indicates that auxin maxima along the provascular ring are correlated with VBs in the WT shoot.

To evaluate whether auxin maxima can control the periodic distribution of VB along the shoot, we formulated a mathematical model for auxin flux across a vascular ring of proliferating cells. This geometry was chosen in concordance with the shoot xylem differentiation pattern (Fig. S1 *B–E*) and following that general, basic pattern, features are preserved among different geometries (31, 32). Previous modeling studies of auxin distribution in the shoot and root meristems have supported the relevance of auxin polar transport in creating auxin maxima (31–34). Based on these studies, our model takes into account auxin polar transport between cells and the apoplast and passive diffusion across the apoplast (*Materials and Methods*). An analysis of the model shows that appropriate asymmetric localization

of efflux carriers is able to elicit auxin maxima (Fig. 1*F*, *SI Text*, and Fig. S2) as expected. Such localization drives fluxes that favor auxin accumulation in groups of cells while depleting auxin in their neighboring cells, thereby producing an unequal auxin distribution along the vascular ring (Fig. 1*G* and Fig. S2*B*). Recently, support for this kind of localization has been reported in both tomato and *Arabidopsis* where lateral polarization of efflux carrier protein PIN1 toward the developing vasculature has been observed (35). Taken together, these data propose efflux carrier localization as promoters of auxin maxima in shoot vascular bundles.

We analyzed whether our model could reproduce the phenotypes of plants with defective auxin polar transport (18, 19). To characterize these phenotypes in further detail, we analyzed the vascular phenotype when 2 genes encoding efflux carrier proteins PIN1 and PIN2 are mutated. *pin1pin2* double mutants showed a more disorganized vascular pattern with an increased number of VBs and xylem differentiated cells compared with the WT control (Fig. S3 *A* and *C*). The xylem differentiation defects were mimicked in plants treated with the auxin transport inhibitor NPA (10 μM, Fig. S3*B*) and are in agreement with previous studies (18, 19). We next evaluated whether the vascular pattern

of plants with defective auxin transport involves a phenotype in auxin maxima distribution. Accordingly, we analyzed the expression pattern of DR5::GUS in plants treated with NPA (10 μM). Our results confirm that auxin maxima are found within VBs, although NPA treatment could also lead to a reduced GUS expression in some VBs (Fig. 1*H*).

We next evaluated this scenario through computational simulations of the model. When the levels of efflux carriers are strongly reduced, auxin distribution becomes disorganized with larger numbers of auxin maxima, which are less strong and can be broader (Fig. 1*I*). Our theoretical analysis revealed that this auxin pattern arose from a slowing-down of the auxin flux dynamics driven by the decrease in efflux transport rates (*SI Text*). For these slow dynamics, initial randomness in the distribution of auxin persists over long times. This result is independent on which mechanism is driving PIN localization. We found the same result in a modified model in which efflux carriers became dynamically reorganized by auxin within the cell (Fig. S4*A*). In this case, we set auxin-dependent cycling dynamics for PIN proteins, as proposed for the shoot apical meristem (31) and took into account that asymmetric endocycling controls the polarization of efflux carriers (36) (*SI Text*). Taken together, our computational results are in agreement with the observed phenotypes for *pin1pin2* mutants and NPA-treated plants, supporting a model in which auxin flow is driving VB patterning.

We next challenged this scenario for VB patterning by using mutants that overproduced auxin. Our model predicted that the number of auxin maxima, and not the levels of auxin, determines the number of VBs because the number of auxin maxima did not change when auxin levels were modified (Fig. 2*A* and *SI Text*). To test this, we examined the vasculature in an auxin-overproducing mutant, *yucca*, which accumulates ≈50% more free indole-3-acetic acid (IAA, the most active auxin) than WT (37). Despite the differences in plant anatomy (37) (Figs. 2*B* and 3*A*), which indicate that the increase in auxin levels in this mutant is significant enough to alter proper plant development, the number of VBs was not modified in *yucca* compared with the WT (Fig. 2 *C* and *D*). As such, our results support the conclusion that auxin levels do not alter the number or arrangement of VBs, as predicted from the model.

It has been reported that BR-deficient mutants have fewer VBs and reduced xylem compared with WT (25, 26, 38). We first analyzed whether this reduction in VBs correlated with a reduction in the number of auxin maxima. We found that DR5:GUS expression in a mutant with null BRI1 receptor activity [*bri1–116*, (39, 40)] was localized only within VBs, confirming that a reduction in VB number involves a reduction in auxin maxima, as well (Fig. S5).

We studied vascular patterning in mutants with impaired BR signaling or synthesis (Table S1, Fig. 3*B*). A comprehensive phenotypic analysis revealed that mutants with reduced BR receptor activity [*bri1–116*, *bri1–301* (39, 40)], signaling [*bin2* (40)], or levels [*cpd* (27)] (Table S1) exhibited a reduced number of VBs compared with WT (Fig. 3 *A*, *D*, *F*, *H*, and *J*). In contrast, transgenic lines or mutations that increased BR signaling [BRI1-GFP overexpression (41–43), *bes1-D* (44), *bzr1-D* (45)] or levels [*DWF4-ox* (46)] (Table S1) led to the formation of a greater number of VBs (Fig. 3 *A*, *C*, *E*, *G*, and *I*). Thus, our results show that either impaired BR synthesis or signaling mutants elicit similar alterations of the vascular pattern, implicating a role for BRs in promoting the formation of VBs (Fig. 4 *A–C*, Fig. S6). Furthermore, chemical inhibition of BR synthesis by using brassinazole (BRZ$_{220}$) or exogenous application of brassinolide (BL, the most active BR) mimicked BR mutants or overexpressing lines, respectively (Fig. S7). Exogenous application of BL in *cpd* mutants restored the number of VBs to WT, whereas BRZ$_{220}$-treated *yucca* plants showed a reduction in the number
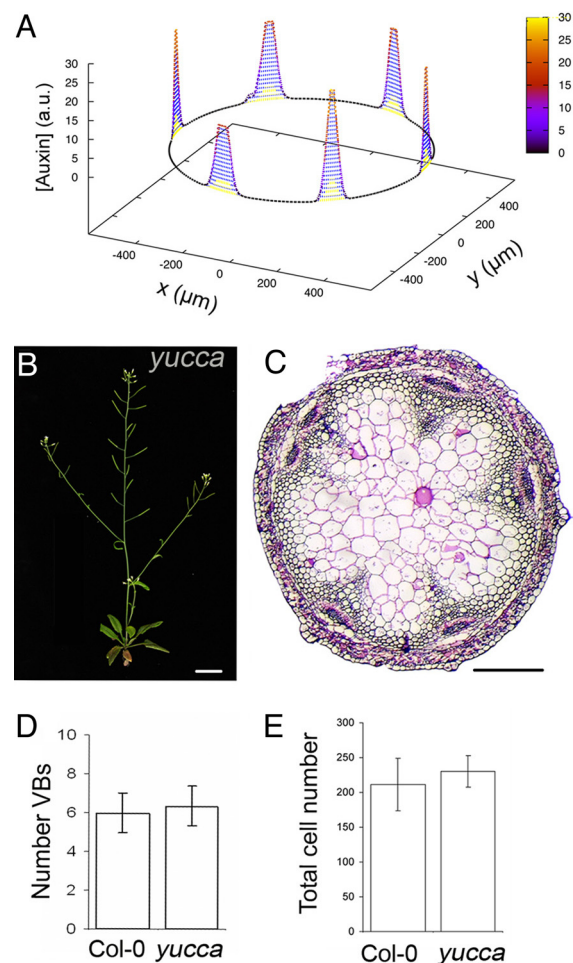

Fig. 2. Auxin levels do not change the number of vascular bundles. (*A*) Auxin levels along a ring of provascular cells when the amount of auxin is 5-fold increased. The reference auxin distribution (shown in Fig. 1*C*) is also plotted (yellow) for comparison. (*B*) Yucca plant. (*C*) Transverse sections of the inflorescence during primary stem development of *yucca* at the base of the inflorescence. (*D*) Average number of VBs for Col-0 WT (*n* = 32) and *yucca* (*n* = 21). (*E*) Average total number of xylem and IF cells (measured as in Fig. 1*F*) along the vascular ring for Col-0 WT (*n* = 18) and *yucca* (*n* = 15). Error bars stand for the standard deviation and *P* > 0.1 in *D* and *E*. (Scale bars: *B*, 2 cm; *C*, 200 μm.)

of VBs (Fig. S7), supporting the specific effects of BRs in the control of vascular pattern.

To elucidate how the number of VBs is modulated by BRs, we analyzed which factors can change the number of auxin maxima in the model. Our study shows that 2 elements control the number of maxima: the average number of cells from one auxin maximum to the subsequent maximum (i.e., the period of the pattern), and the total number of cells when the auxin pattern emerges (Fig. S4 *B–D*; *SI Text*). Thus, if auxin maxima arise closer to each other in terms of cell numbers, more maxima would be formed within a ring of a fixed-cell number. Alternatively, higher numbers of auxin maxima arise as more cells compose the ring when the pattern is being settled down (Fig. 4 *D* and *E* and Fig. 1*F*).

We first evaluated whether the period of the pattern is strongly altered in BR mutants. To this end, we measured the number of cells forming each vascular unit across the ring, i.e., the number of procambial and clockwise adjacent contiguous IF cells at the base of the vascular ring for each VB (Fig. 1 *A* and *B*). We observed that procambial cell division occurs centripetally,
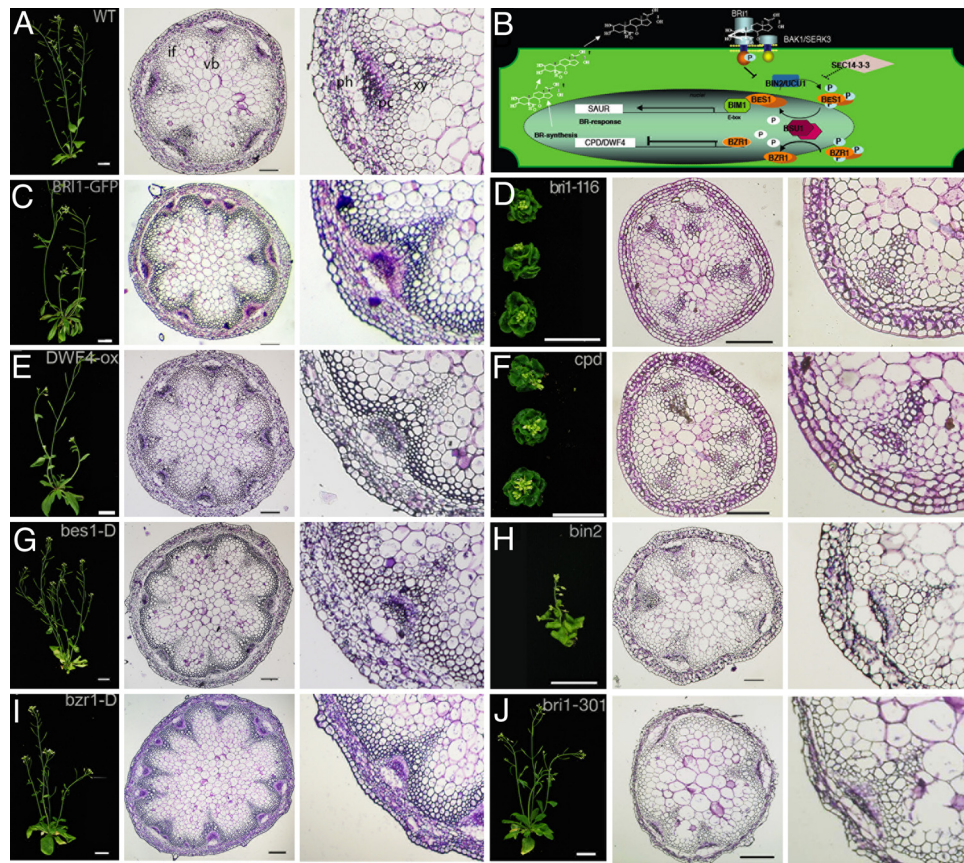
Fig. 3. BR-signaling mutants modulate the number of vascular bundles. (*A*, *C–J*) From left to right: plant phenotype, cross section at the base of the inflorescence, and a detail of a VB for the WT Col-0 plants (*A*), mutants with enhanced BR-signaling and/or synthesis *BRI1-GFP* (*C*), *DWF4-ox* (*E*), *bes1-D* (*G*), and *bzr1-D* (*I*), respectively. The same is shown for mutants with reduced BR-synthesis and/or signaling *bri1–116* (*D*), *cpd* (*F*), *bin2* (*H*), and *bri1–301* (*J*). (*B*) Schematic representation of BR signaling pathway showing BR receptor BRI1 at the plasma membrane and downstream signaling component BIN2, a negative regulator that controls the activities of transcription factors BES1 and BZR1. Coordinated action of BZR1, which negatively regulates the expression of BR-synthesis genes (CPD and DWARF4), and BES1 transcription factor maintain BR-signaling in tune. vb, vascular bundle; if, interfascicular fiber; pc, procambium; ph, phloem; xy, xylem. (Scale bars: 2 cm for plants, 100 μm for stem sections except for *J*, 200 μm.)

leading to the formation of xylem cells in the VB in such a way that each procambial cell correlated with the first differentiated xylem cell (Fig. 1*B*). To elicit changes in the periodic pattern that would explain the modulation of VB number, we reasoned that fewer cells per vascular unit must be found in gain-of-function mutants, whereas an increase in cells per unit must occur in loss-of-function mutants. Our analysis revealed that the number of xylem and IF cells per vascular unit was similar for gain-of-function mutants and the WT, whereas it decreased slightly for loss-of-function mutants (Fig. 4*F* and Fig. S6). These results show that modulation of VB number is not fixed by changes in the periodicity of the pattern.

We next computed the total number of cells, xylem and IF, at the base of the vascular ring in the BR mutants (Fig. 1 *A* and *B*). According to our previous results on the average cell number per vascular unit, we expected the total number of cells to increase in gain-of-function BR mutants and to be reduced in loss-of-function BR mutants. The analysis confirmed this and revealed a dramatic increase in the number of cells in the vascular ring of gain-of-function BR-signaling mutants, whereas loss-of-function BR-mutants had fewer cells than the wild type (Fig. 4*G* and Fig. S6). Similar features were observed in apical regions of the inflorescence stem (Fig. S1 *F* and *G*). Note that an increase in the number of cells forming the vascular ring in BR gain-of-function mutants was not translated to an increase of the stem diameter, as demonstrated by the extreme phenotype of *bzr1-D* mutants (Fig. 4 *G* and *I*). Interestingly, we found that both BR

gain-of-function and loss-of-function mutants show a vascular pattern with VBs spaced shorter distances and show smaller IF cells (Fig. S8).

We found a statistically significant correlation between the number of VBs and the total number of cells in the vascular ring (Fig. 4*H*), consistent with the predictions of the model. Moreover, supporting the different roles of BRs and auxin polar transport in our model for vascular patterning, we did not find such a correlation in plants with defective auxin efflux polar transport (Fig. S3 *D* and *E*). The specific role for BRs in the patterning process is further supported by the phenotype of auxin-overproducing *yucca* mutants, which had a similar number of vascular ring cells compared with the WT (Fig. 2*E* and Fig. S6).

Our results indicate that BR-induced changes in provascular cell number are crucial for modulation of VB number and suggest a role for BRs in controlling procambial cell divisions. Previous studies have documented the role of BRs in promoting cell expansion, but little information has been published concerning a role for BRs in cell division. These distinct functions of BRs, in cell expansion in vegetative shoot tissues or in the control of cell division during vascular pattern formation, may be the result of cell-type specific BR signaling conferred by the BRL1 and BRL3 receptors, which are expressed specifically in vascular cells (25). Unlike BRI1, which is ubiquitously expressed and known to promote cell expansion, the downstream signaling components for BRL1 and BRL3 await to be identified.

SYSTEMS BIOLOGY

Fig. 4. BRs control the number of cells in the vascular ring. (*A* and *B*) Frequency of number of VBs for BR-loss-of-function mutants *bri1–116* (crosses) and *cpd* (triangles) (*A*) and BR-gain-of-function mutants *DWF4-ox* (triangles), *bes1-D* (squares), and *bzr1-D* (diamonds) (*B*) compared with Col-0 WT (black circles). Lines are used as a guide to the eye. (*C* and *I*) Average number of VBs (*C*) and diameter (*I*) at the base of the inflorescence for each mutant genotype. In *C*, *I*, *F*, and *G*, error bars represent the standard deviation, asterisks stand for *P*-values <0.01 (the data set from each genotype is compared with the WT data; see *Materials and Methods*) and sizes of datasets are found in Table S2 and Table S3. Fig. S6 shows the boxplots of all data in *C*, *I*, *F*, and *G*. In *C*, *bri1–301* has a *P* value <0.05. (*D* and *E*) Simulation results for the auxin concentration along a ring of few (*D*) and many (*E*) cells, mimicking BR-loss- and gain-of-function mutants, respectively. Parameter values as in Fig. 1*F* with (*D*) $N_i = 80$, $N_F = 100$ and (*E*) $N_i = 135$, $N_F = 250$ cells, and average diameter (*I*) for *bri1–116* and *bzr1-D* is being used. (*F* and *G*) Average number of xylem cells within a VB plus the clockwise adjacent interfascicular cells (*F*), and average total number of cells along the vascular ring for BR-mutant genotypes and Col-0 WT (*G*). (*H*) Total number of differentiated cells along the vascular ring as a function of the number of vascular bundles in the stem for each cross section analyzed for different BR-mutant genotypes (*bri1–116*, *cpd*, *DWF4-ox*, and *bzr1-D*) and Col-0 WT (same symbol code used as in *A* and *B*). Linear fit (R² = 0.86) shown.

In summary, we have used mathematical modeling to evaluate the roles of the plant hormones auxin and BRs in the establishment of shoot vascular architecture. The model made specific predictions, which we have addressed experimentally and that together provide a framework for understanding the action of auxin and BRs in shoot vascular patterning. Our results reveal that BRs serve as a promoting signal for the number of cells in the provascular ring and are consistent with auxin maxima, established by asymmetric auxin polar transport and not dependent on changes in auxin levels, acting to position the vascular bundles across the vascular ring. As such, the coordinated action of these 2 plant hormones is required to establish the periodic arrangement of vascular bundles in the shoot.

Our results point at auxin maxima as a common element between lateral organ positioning and shoot vasculature formation and show that early xylem-differentiating cells are observed at the shoot apex concurrent with lateral organ primordia outgrowth (Fig. S1). Thus, it is tempting to propose that early

signaling events at the shoot apex control the initiation of shoot vascular pattern in the plant, although whether these arise from central and/or peripheral zones of the meristem and whether these are linked with organ primordia positioning remains to be investigated. Future studies using local auxin and BRs response during vascular primordia initiation and differentiation may reveal additional interactions of these two signaling pathways underlying vascular-bundle patterning and plant development.

Materials and Methods

Plant Material and Growth Conditions. *Arabidopsis* Columbia (Col-0) ecotype was the wild type and all mutant plants described in Table S1 were derived from this accession. Seeds were surface-sterilized in 35% sodium hypochloride, vernalized at 4 °C for 48 h, and germinated on plates containing Murashige and Skoog (MS) salt mixture. Plants were grown under long-day photoperiodic conditions. Pharmacological treatments were performed in plants grown in magenta boxes containing MS media supplemented with 10 nM BL ($C_{28}H_{48}O_6$; Wako), 5 µM BRZ$_{220}$, and 10 µM NPA respectively. The shoot inflorescence stems were cut from plants at 12 to 22 days after bolting.

Histology and Microscopy. *Arabidopsis* stems were fixed overnight in 3.7% (vol/vol) formaldehyde. Samples were dehydrated with a graded series of ethanol/Histoclear (3:1, 1:1, 1:3, histoclear) and embedded in paraplast (Sigma). Transverse stem sections (6 μm) were made by using a Microtome (Jung-Autocut, Leica). Sections were stained with 0.1% Toluidine blue or Phloroglucinol solution, and visualized by using an Axiophot (Zeiss) microscope. GUS activity and Historesin embedding were performed as reported previously (25).

Quantitative Vascular Analysis: Measurement Settings. Quantification of vascular parameters (stem diameters, number of cells, and IF length) was performed by using ImageJ (http://rsb.info.nih.gov/ij/). Two orthogonal diameters were measured along the directions of maximal or minimal length and the mean value was used. Similar conclusions are obtained if the pith diameter is included in the analysis (Fig. S8). To ensure measurements were made on stationary conditions for bundle number and stem diameter, we analyzed WT sections at different times after bolting at the base of the inflorescence. A Wilcoxon Mann–Whitney rank sum statistical test was used to evaluate whether each mutant genotype dataset followed the same distribution as the data from WT plants (see *SI Text*).

Mathematical Modeling. We set a model of auxin dynamics across a ring of vascular cells and the surrounding apoplast in which stochastic cell division is incorporated (*SI Text*). The model can evaluate the effect of changes in efflux carriers, cell number, and dynamics on auxin distribution. Both active polar transport and diffusion is taken into account (31). The model reads (see *SI Text* for details):

$$\frac{dA_i}{dt} = \varepsilon \sum_{j \in n(i)} I_{ij} a_j - \varepsilon \sum_{j \in n(i)} E_{ij} A_i$$

$$\frac{da_i}{dt} = \sum_{j \in N(i)} E_{ji} A_j - \sum_{j \in N(i)} I_{ji} a_i + D \nabla_i^2 a_i$$

where A_i and a_i stand for auxin concentrations in cell i and in the apoplast i, respectively, and space has been discretized (Fig. S2 *A*). E_{ij} and I_{ij} are the efflux and influx transport coefficients or permeabilities between cell i and apoplast j, which depend on the level of efflux and influx carriers, respectively. Influx and efflux permeabilities are detailed in *SI Text*. D represents the effective diffusion rate along the apoplast. ε is the ratio between the linear size of the apoplast and the linear size of cells. $n(i)$ runs over the apoplast neighboring cell i, while $N(i)$ runs over cells surrounding apoplast i. We included cell proliferation dynamics and considered that tissue cell proliferation occurs at a slower time scale than auxin dynamics. Cells divided at random and, as a first approximation, we assumed they reached their final growth very rapidly (47), expanding the provascular ring and preserving its circular shape (Fig. S9).

1. Essau K (1965) *Plant Anatomy* (Wiley, New York), 2nd Ed.
2. Fisher K, Turner S (2007) PXY, a receptor-like kinase essential for maintaining polarity during plant vascular-tissue development. *Curr Biol* 17:1061–1066.
3. Rolland-Lagan AG, Prusinkiewicz P (2005) Reviewing models of auxin canalization in the context of leaf vein pattern formation in Arabidopsis. *Plant J* 44:854–865.
4. Sachs T (1981) The control of the patterned differentiation of vascular tissues. *Adv Bot Res* 9:151–262.
5. Scarpella E, Marcos D, Friml J, Berleth T (2006) Control of leaf vascular patterning by polar auxin transport. *Genes Dev* 20:1015–1027.
6. Jurgens G (2001) Apical-basal pattern formation in *Arabidopsis* embryogenesis. *EMBO J* 20:3609–3616.
7. Berleth T, Mattsson J (2000) Vascular development: Tracing signals along veins. *Curr Opin Plant Biol* 3:406–411.
8. Sieburth LE, Deyholos MK (2006) Vascular development: The long and winding road. *Curr Opin Plant Biol* 9:48–54.
9. Zhong R, Taylor JJ, Ye ZH (1997) Disruption of interfascicular fiber differentiation in an *Arabidopsis* mutant. *Plant Cell* 9:2159–2170.
10. Carland FM, et al. (1999) Genetic regulation of vascular tissue patterning in *Arabidopsis*. *Plant Cell* 11(11):2123–2137.
11. Mahonen AP, et al. (2000) A novel two-component hybrid molecule regulates vascular morphogenesis of the *Arabidopsis* root. *Genes Dev* 14:2938–2943.
12. Clay NK, Nelson T (2002) VH1, a provascular cell-specific receptor kinase that influences leaf cell patterns in *Arabidopsis*. *Plant Cell* 14:2707–2722.
13. Berleth T, Sachs T (2001) Plant morphogenesis: Long-distance coordination and local patterning. *Curr Opin Plant Biol* 4:57–62.
14. Fukuda H (1997) Tracheary element differentiation. *Plant Cell* 9:1147–1156.
15. Uggla C, Moritz T, Sandberg G, Sundberg B (1996) Auxin as a positional signal in pattern formation in plants. *Proc Natl Acad Sci USA* 93:9282–9286.
16. Mattsson J, Ckurshumova W, Berleth T (2003) Auxin signaling in *Arabidopsis* leaf vascular development. *Plant Physiol* 131:1327–1339.
17. Wenzel CL, Schuetz M, Yu Q, Mattsson J (2007) Dynamics of MONOPTEROS and PIN-FORMED1 expression during leaf vein pattern formation in *Arabidopsis thaliana*. *Plant J* 49:387–398.
18. Galweiler L, et al. (1998) Regulation of polar auxin transport by AtPIN1 in *Arabidopsis* vascular tissue. *Science* 282:2226–2230.
19. Mattsson J, Sung ZR, Berleth T (1999) Responses of plant vascular systems to auxin transport inhibition. *Development* 126:2979–2991.
20. Vert G, Walcher CL, Chory J, Nemhauser JL (2008) Integration of auxin and brassinosteroid pathways by Auxin Response Factor 2. *Proc Natl Acad Sci USA* 105:9829–9834.
21. Fukuda H, Ito M, Sugiyama M, Komamine A (1994) Mechanisms of the proliferation and differentiation of plant cells in cell culture systems. *Int J Dev Biol* 38:287–299.
22. Nagata N, Asami T, Yoshida S (2001) Brassinazole, an inhibitor of brassinosteroid biosynthesis, inhibits development of secondary xylem in cress plants (*Lepidium sativum*). *Plant Cell Physiol* 42:1006–1011.
23. Yamamoto R, et al. (2001) Brassinosteroid levels increase drastically prior to morphogenesis of tracheary elements. *Plant Physiol* 125:556–563.
24. Nakamura A, et al. (2006) The role of OsBRI1 and its homologous genes, OsBRL1 and OsBRL3, in rice. *Plant Physiol* 140:580–590.
25. Caño-Delgado A, et al. (2004) BRL1 and BRL3 are novel brassinosteroid receptors that function in vascular differentiation in *Arabidopsis*. *Development* 131(21):5341–5351.
26. Choe S, et al. (1999) The *Arabidopsis* dwf7/ste1 mutant is defective in the delta7 sterol C-5 desaturation step leading to brassinosteroid biosynthesis. *Plant Cell* 11:207–221.
27. Szekeres M, et al. (1996) Brassinosteroids rescue the deficiency of CYP90, a cytochrome P450, controlling cell elongation and de-etiolation in *Arabidopsis*. *Cell* 85:171–182.
28. Benková E, et al. (2003) Local, efflux-dependent auxin gradients as a common module for plant organ formation. *Cell* 115:591–602.
29. Reinhardt D, et al. (2003) Regulation of phyllotaxis by polar auxin transport. *Nature* 426:255–260.
30. Ulmasov T, Murfett J, Hagen G, Guilfoyle TJ (1997) Aux/IAA proteins repress expression of reporter genes containing natural and highly active synthetic auxin response elements. *Plant Cell* 9:1963–1971.
31. Jonsson H, Heisler MG, Shapiro BE, Meyerowitz EM, Mjolsness E (2006) An auxin-driven polarized transport model for phyllotaxis. *Proc Natl Acad Sci USA* 103:1633–1638.
32. Smith RS, et al. (2006) A plausible model of phyllotaxis. *Proc Natl Acad Sci USA* 103:1301–1306.
33. de Reuille PB, et al. (2006) Computer simulations reveal properties of the cell-cell signaling network at the shoot apex in *Arabidopsis*. *Proc Natl Acad Sci USA* 103:1627–1632.
34. Grieneisen VA, Xu J, Maree AF, Hogeweg P, Scheres B (2007) Auxin transport is sufficient to generate a maximum and gradient guiding root growth. *Nature* 449:1008–1013.
35. Bayer EM, et al. (2009) Integration of transport-based models for phyllotaxis and midvein formation. *Genes Dev* 23:373–384.
36. Dhonukshe P, et al. (2008) Generation of cell polarity in plants links endocytosis, auxin distribution and cell fate decisions. *Nature* 456:962–966.
37. Zhao Y, et al. (2001) A role for flavin monooxygenase-like enzymes in auxin biosynthesis. *Science* 291:306–309.
38. Savaldi-Goldstein S, Peto C, Chory J (2007) The epidermis both drives and restricts plant shoot growth. *Nature* 446:199–202.
39. Li J, Chory J (1997) A putative leucine-rich repeat receptor kinase involved in brassinosteroid signal transduction. *Cell* 90:929–938.
40. Li J, Nam KH, Vafeados D, Chory J (2001) BIN2, a new brassinosteroid-insensitive locus in *Arabidopsis*. *Plant Cell* 127:14–22.
41. Friedrichsen DM, Joazeiro CA, Li J, Hunter T, Chory J (2000) Brassinosteroid-insensitive-1 is a ubiquitously expressed leucine-rich repeat receptor serine/threonine kinase. *Plant Physiol* 123:1247–1256.
42. Kinoshita T, et al. (2005) Binding of brassinosteroids to the extracellular domain of plant receptor kinase BRI1. *Nature* 433:167–171.
43. Wang ZY, Seto H, Fujioka S, Yoshida S, Chory J (2001) BRI1 is a critical component of a plasma-membrane receptor for plant steroids. *Nature* 410:380–383.
44. Yin Y, et al. (2002) BES1 accumulates in the nucleus in response to brassinosteroids to regulate gene expression and promote stem elongation. *Cell* 109:181–191.
45. Wang ZY, et al. (2002) Nuclear-localized BZR1 mediates brassinosteroid-induced growth and feedback suppression of brassinosteroid biosynthesis. *Dev Cell* 2:505–513.
46. Choe S, et al. (2001) Overexpression of DWARF4 in the brassinosteroid biosynthetic pathway results in increased vegetative growth and seed yield in *Arabidopsis*. *Plant J* 26:573–582.
47. Ibañes M, Kawakami Y, Rasskin-Gutman D, Belmonte JC (2006) Cell lineage transport: A mechanism for molecular gradient formation. *Mol Syst Biol* 2:57.

SYSTEMS BIOLOGY

Ibañes et al.